International Journal of Innovative Computing, Information and Control
Volume **19**, Number **2**, April **2023**

ICIC International ©2023 ISSN 1349-4198
pp. **307–323**

SIMULATED RESPONSE ANALYSIS: MODELLING A WHEELCHAIR-OCCUPANT SYSTEM SUBJECTED TO VIBRATION

Pongtep Weerapong[1,2], Kotaro Hashikura[3], Md Abdus Samad Kamal[3]
Iwanori Murakami[3] and Kou Yamada[3]

[1]Department of Production Technology
Faculty of Industrial Technology
Nakhon Si Thammarat Rajabhat University
M4 Tha-Ngow Subdistrict, Maung District, Nakhon Si Thammarat 80280, Thailand
pongtap_wee@nstru.ac.th

[2]Graduate School of Science and Technology
[3]Division of Mechanical Science and Technology
Gunma University
1-5-1 Tenjincho, Kiryu 376-8515, Japan
{ t202b007; k-hashikura; maskamal; murakami; yamada }@gunma-u.ac.jp

Received June 2022; revised October 2022

Abstract. *This paper discusses an approach to evaluating the prediction accuracy of the output from a wheelchair-occupant simulation model in comparison with real-world experimental results. Different model setups, in which the wheelchair's occupant is supported on three types of seat cushions, are formulated with the model subjected to low-frequency vibration waves arising from the interaction between wheelchair tires and ground profile. The model's output, in terms of displacement response of the wheelchair and its occupant's body parts, is analyzed and validated for goodness-of-fit against the results of well-defined published papers. The analysis reveals that the occupant's torso receives the largest impact from vibration causing the organ to exhibit maximum displacement; and the foam-based cushion performs the best in helping to dampen the amplitude of displacement responses.*

Keywords: Simulated response analysis, Wheelchair-occupant system, Vibration, Seat cushion, Transmissibility, Mathematical model, Displacement response, Goodness-of-fit

1. **Introduction.** The World Health Organization has put the global percentage of wheelchair users at 1.0 percent of world population [1]. Inevitably, wheelchair riders are subjected to the impact of vibration associated with their daily wheelchair operation, which can cause physical discomfort ranging from minor symptoms to severe, chronic illnesses [2, 3]. Griffin [4] and Gao et al. [5] found that sustained exposure to vibration on the wheelchair can result in harm to the occupant's anatomy such as the head, neck, torso, and pelvis. Among the efforts to reduce such harmful vibration in modern wheelchair production, three directions of design approach are generally favored by investigators: (i) Modification of wheel shape and profile [3, 6], (ii) Redesign of wheelchair component parts using newly-engineered materials [7, 8] and (iii) Modification of the seat cushion [9, 10].

Considering the effectiveness as well as the cost of the said approaches, the third option should be the most economical and accessible. Modifying the seat cushion entails a decision on the choice of seat material to use – a decision that can be made through experiments with actual cushion products, or through computer simulation of the potential materials. It is to the latter area of investigation that the authors aim to make a

DOI: 10.24507/ijicic.19.02.307

contribution through formulating an effective simulation model [11]. With this approach, the dynamic behavior of the wheelchair cushions can be characterized using laboratory equipment without the need for a human subject. Early in our literature review, we found that Garcia-Mendez et al. [9] conducted a set of experiments by placing human subjects on actual moving wheelchairs with seven types of seat cushion in order to study the vibration transmissibility of the seat assembly. Therefore, with computer simulation in mind, we created a wheelchair-occupant system with nine degrees of freedom (9-DOF) which was employed to study the vibration transmissibility of the seat cushion materials – see Weerapong et al. [12, 13]. Results from the initial 9-DOF model were found to corroborate well with the actual experimental results reported by Garcia-Mendez et al. [9]. From this initial model, we chose to extend it by isolating the previous model's wheels from its suspension, thereby adding two additional dimensions to the setup. The greater dimensionality of the current 11-DOF model was to enable direct analyses of the forces acting on the seat cushion – an improvement that was lacking in the previous 9-DOF model.

In terms of the seat transmissibility and displacement ratio of the occupant's body parts [14], the results obtained from the 11-DOF model exhibited a much-improved correlation with the reported findings of Garcia-Mendez et al. [9]. This was indicated by the high ratios of the goodness-of-fit of the seat transmissibility values between the actual experiments and the simulated output of the model; some as high as 84[%] were obtained, as shown in Table 4. This model may be used by designers or clinicians to conveniently predict the requirements of the cushion materials so that the assembled wheelchair will provide its human occupant with greater levels of ride comfort. The seat materials chosen for our model are commercially available products in three categories: air-, gel- and foam-based cushions. Wider ranges of material type may be simulated on the model where necessary provided their stiffness and damping parameters can be determined for input into the model.

This paper is organized in 5 sections. Section 2 analyzes the wheelchair and occupant regarding properties of human tissue, spring and damper, and defines the force vectors upon the masses in the free body diagram. Section 3 has the model's equation of motions (EOMs) rearranged, using Fourier transformation and Euler's formula, into matrices containing equations and frequency response functions. Section 4 concerns the evaluation and validation of the wheelchair-occupant model, and application of transmissibility and the displacement responses to assess the prediction accuracy of the model. Section 5 delivers concluding remarks.

Notations

m	Mass, (kg).	k	Stiffness of the spring, (N/m).
c	Damping coefficient, (Ns/m).	$[M]$	Mass matrix.
y	Displacement, (mm).	$[C]$	Damping matrix.
t	Time, (s).	$[K]$	Stiffness matrix.
ω	Frequency, (rad/s).	$[K_0]$	Input stiffness matrix.
i	$\sqrt{-1}$, Index.	$[C_0]$	Input damping matrix.
T	Transmissibility.	$\{F\}$	Input force excitation vector.
$\{y_0\}, \{\dot{y}_0\}$	Displacement and velocity vectors of excitation.		
$\{y\}, \{\dot{y}\}, \{\ddot{y}\}$	Displacement, velocity and acceleration vectors of response.		

2. **Analysis of Lumped Mechanical System.** The construction of our model, consisting of a wheelchair and its occupant, is outlined in Figure 1. The wheelchair, with four degrees of freedom, is represented by four blocks: (i) the seat, padded with a cushion of negligible mass, denoted by m_8; (ii) the chair frame, denoted by m_9; (iii) the front

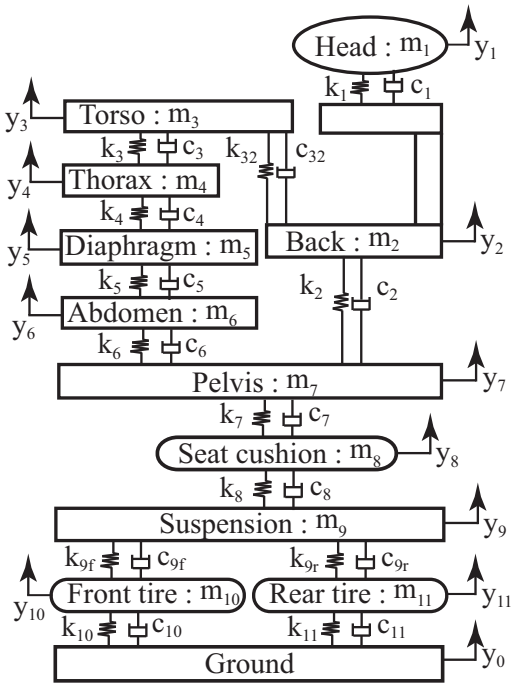

FIGURE 1. Eleven lumped parameter model of wheelchair-occupant assembly

TABLE 1. Parameter values of manual wheelchair [9, 15]

Mass[M] (kg)	Damping constant[C] (N/m/sec)	Spring constant[K] (N/m)
$m_{11} = 1.6$	$c_{11} = 500$	$k_{11} = 6000$
$m_{10} = 1.0$	$c_{10} = 500$	$k_{10} = 60000$
$m_9 = 15$	$c_{9f} = 700$	$k_{9f} = 13400$
	$c_{9r} = 700$	$k_{9r} = 74600$
$m_8 = 1.5$	$c_{2a} = 834$	$k_{2a} = 94220$
	$c_{2b} = 571$	$k_{2b} = 39970$
	$c_{2c} = 1507$	$k_{2c} = 174900$
Input magnitude vibration, $Y_0 = 5.00$ mm.		

f and r denote the parameter value for suspension f, for front; r, for rear. a, b, and c denote the cushion types: a, for air-based (Roho High Profile); b, for gel-based (Jay J2 Deep Contour); and c, for foam-based (Zoombang Protective Gear with Foam).

tires, denoted by m_{10}; and (iv), the rear tires, m_{11}. Wheelchair characteristics, listed in Table 1, have been obtained from published international standards, and whose values have been validated through calculations using the EOMs of our model as described in Section 4.1 below. The occupant is treated as a 7-DOF frame emulating the work of Liang and Chiang [16], which employed an idealized anatomy of the sitting human body whose parts are isolated at the joints where relative movements are allowed, and the parts considered as lumped masses. The seven blocks, comprising head (m_1), back (m_2), torso (m_3), thorax (m_4), diaphragm (m_5), abdomen (m_6), and pelvis (m_7), are connected by springs and dampers, representing the resilient characteristics of the connective tissues between the components. The parameter values of such human tissues, obtained from various published studies of anatomical subsystems, are listed in Table 2. The seated occupant has its lower segment(s) supported by the seat cushion, while its upper segments unsupported by a backrest. The wheelchair is modeled as a typical manual device for use

TABLE 2. Parameter values of occupant model [16]

Mass[M] (kg)	Damping constant[C] (N/m/sec)	Spring constant[K] (N/m)
$m_7 = 27.7$	$c_7 = 378$	$k_7 = 25500$
$m_6 = 6.02$	$c_6 = 298$	$k_6 = 894.1$
$m_5 = 0.46$	$c_5 = 298$	$k_5 = 894.1$
$m_4 = 1.38$	$c_4 = 298$	$k_4 = 894.1$
$m_3 = 33.33$	$c_3 = 298$	$k_3 = 894.1$
	$c_{32} = 3651$	$k_{32} = 53640$
$m_2 = 6.94$	$c_2 = 3651$	$k_2 = 53640$
$m_1 = 5.5$	$c_1 = 3651$	$k_1 = 53640$

on typical urban traffic surfaces. Input vibrations on it are limited to those coming from the sinusoidal functions of the springs and dampers on its tires and emanating through the seat cushion to the occupant's body. Amplitude of the input wave is set at 0.005[m]. The real-world vibration waves through the wheelchair foot support are ignored in the simulation as they are negligibly small in magnitude and will not affect the occupant's trunk. The wheelchair-occupant system is shown in cross-section having eleven blocks of mass, denoted by m_k, $(k = 1, 2, \ldots, 11)$, that are connected in pairs with a spring and a dashpot whose respective stiffness and damping coefficients, k_k and c_k, are listed in Tables 1 and 2.

3. **Assumptions and Formulation.** The dynamics of the wheelchair-occupant assembly is treated as a system in steady state where forces acting on its components are externally originated. The governing equations of motion (EOMs) of the system were derived from the FBD in Figure 1 through the application of Newton's Third Law of Motion. After appropriate mathematical adjustment, the EOMs were transformed into linear polynomials. Thus, the eleven degrees of freedom gave rise to eleven EOMs as explained below.

3.1. **Model description of the 11-DOF.** The mass, stiffness and damping characteristics of the model are expressed as 11 by 11 matrices denoted by $[M]$, $[K]$ and $[C]$. Each matrix, upon being multiplied with $\{\ddot{y}(t)\}$, $\{\dot{y}(t)\}$ and $\{y(t)\}$ yields acceleration, velocity and displacement vectors of the system – all of which being dependent on the characteristics of force F. $\{F\}$ is the harmonic excitation force vectors; ω represents the excitation frequency; while $[K_0]$ and $[C_0]$, the stiffness and damping matrices at excitation; and $\{y_0(t)\}$ and $\{\dot{y}_0(t)\}$, the resulting displacement and velocity vectors upon excitation. Relationships of these variables can be expressed in matrix and vector forms as shown in Equations (1) and (2):

$$[M]\{\ddot{y}(t)\} + [C]\{\dot{y}(t)\} + [K]\{y(t)\} = \{F\}\sin\omega t, \tag{1}$$

$$\{F\} = [K_0]\{y_0(t)\} + [C_0]\{\dot{y}_0(t)\}. \tag{2}$$

3.1.1. *Derivation of EOMs in matrix form.* The governing EOM for each mass consists of its inertia term and forces exerted on it by the stiffnesses and dampers due to the relative motion of the connected masses. In an EOM, each of the variables – including $[M] = m_k$, $[K] = k_k$, $[C] = c_k$, $\{y(t)\} = y_k$, $\{\dot{y}(t)\} = \dot{y}_k$ and $\{\ddot{y}(t)\} = \ddot{y}_k$ – is subscripted with a number from 1 to 11 that represents an assigned component (i.e., $(k = 1, 2, \ldots, 11)$ whereby 1 to 7 denote the body parts; and 8 to 11 being the wheelchair components). In addition, $\{y_0(t)\}$ and $\{\dot{y}_0(t)\}$ respectively refer to the input displacement and velocity

vector of the tire contact points to the floor. As the floor surface will cause the tires to compress, $y_0(t)$ and $\dot{y}_0(t)$ are, respectively, the amplitude of input displacement excitation and circular frequency of this displacement applied at the tire contact points. The EOMs and their mathematical notations are shown as Equations (3) to (32).

The elements of these matrices are obtained from the EOMs. With the mass matrix, $[M] \in R^{11\times 11}$, its elements are zero except those on its diagonal, and it is written as

$$[M] = \begin{bmatrix} m_1 & 0 & 0 & 0 & 0 & 0 & 0 & 0 & 0 & 0 & 0 \\ 0 & m_2 & 0 & 0 & 0 & 0 & 0 & 0 & 0 & 0 & 0 \\ 0 & 0 & m_3 & 0 & 0 & 0 & 0 & 0 & 0 & 0 & 0 \\ 0 & 0 & 0 & m_4 & 0 & 0 & 0 & 0 & 0 & 0 & 0 \\ 0 & 0 & 0 & 0 & m_5 & 0 & 0 & 0 & 0 & 0 & 0 \\ 0 & 0 & 0 & 0 & 0 & m_6 & 0 & 0 & 0 & 0 & 0 \\ 0 & 0 & 0 & 0 & 0 & 0 & m_7 & 0 & 0 & 0 & 0 \\ 0 & 0 & 0 & 0 & 0 & 0 & 0 & m_8 & 0 & 0 & 0 \\ 0 & 0 & 0 & 0 & 0 & 0 & 0 & 0 & m_9 & 0 & 0 \\ 0 & 0 & 0 & 0 & 0 & 0 & 0 & 0 & 0 & m_{10} & 0 \\ 0 & 0 & 0 & 0 & 0 & 0 & 0 & 0 & 0 & 0 & m_{11} \end{bmatrix}. \tag{3}$$

$[C] \in R^{11\times 11}$ is the damping matrix and written as

$$[C] = \begin{bmatrix} c_1 & -c_1 & 0 & 0 & 0 & 0 & 0 & 0 & 0 & 0 & 0 \\ -c_1 & A & -c_{32} & 0 & 0 & -c_2 & 0 & 0 & 0 & 0 & 0 \\ 0 & -c_{32} & B & -c_3 & 0 & 0 & 0 & 0 & 0 & 0 & 0 \\ 0 & 0 & -c_3 & C & -c_4 & 0 & 0 & 0 & 0 & 0 & 0 \\ 0 & 0 & 0 & -c_4 & D & -c_5 & 0 & 0 & 0 & 0 & 0 \\ 0 & 0 & 0 & 0 & -c_5 & E & -c_6 & 0 & 0 & 0 & 0 \\ 0 & -c_2 & 0 & 0 & 0 & -c_6 & F & -c_7 & 0 & 0 & 0 \\ 0 & 0 & 0 & 0 & 0 & 0 & -c_7 & G & -c_8 & 0 & 0 \\ 0 & 0 & 0 & 0 & 0 & 0 & 0 & -c_8 & H & -c_{9f} & -c_{9r} \\ 0 & 0 & 0 & 0 & 0 & 0 & 0 & 0 & -c_{9f} & I & 0 \\ 0 & 0 & 0 & 0 & 0 & 0 & 0 & 0 & -c_{9r} & 0 & J \end{bmatrix}, \tag{4}$$

where

$$A = c_1 + c_2 + c_{32}, \tag{5}$$

$$B = c_{32} + c_3, \tag{6}$$

$$C = c_3 + c_4, \tag{7}$$

$$D = c_4 + c_5, \tag{8}$$

$$E = c_5 + c_6, \tag{9}$$

$$F = c_6 + c_7 + c_2, \tag{10}$$

$$G = c_7 + c_8, \tag{11}$$

$$H = c_8 + c_{9f} + c_{9r}, \tag{12}$$

$$I = c_{9f} + c_{10}, \tag{13}$$

and

$$J = c_{9r} + c_{11}. \tag{14}$$

A to J represent variables in the positions of $[C]$ caused by the sum of the damping constant (c_k) as shown in Equations (5) to (14).

$[K] \in R^{11\times 11}$ is the stiffness matrix and written as

$$[K] = \begin{bmatrix} k_1 & -k_1 & 0 & 0 & 0 & 0 & 0 & 0 & 0 & 0 & 0 \\ -k_1 & K & -k_{32} & 0 & 0 & -k_2 & 0 & 0 & 0 & 0 & 0 \\ 0 & -k_{32} & L & -k_3 & 0 & 0 & 0 & 0 & 0 & 0 & 0 \\ 0 & 0 & -k_3 & M & -k_4 & 0 & 0 & 0 & 0 & 0 & 0 \\ 0 & 0 & 0 & -k_4 & N & -k_5 & 0 & 0 & 0 & 0 & 0 \\ 0 & 0 & 0 & 0 & -k_5 & O & -k_6 & 0 & 0 & 0 & 0 \\ 0 & -k_2 & 0 & 0 & 0 & -k_6 & P & -k_7 & 0 & 0 & 0 \\ 0 & 0 & 0 & 0 & 0 & 0 & -k_7 & Q & -k_8 & 0 & 0 \\ 0 & 0 & 0 & 0 & 0 & 0 & 0 & -k_8 & R & -k_{9f} & -k_{9r} \\ 0 & 0 & 0 & 0 & 0 & 0 & 0 & 0 & -k_{9f} & S & 0 \\ 0 & 0 & 0 & 0 & 0 & 0 & 0 & 0 & -k_{9r} & 0 & T \end{bmatrix}, \tag{15}$$

where

$$K = k_1 + k_2 + k_{32}, \tag{16}$$

$$L = k_{32} + k_3, \tag{17}$$

$$M = k_3 + k_4, \tag{18}$$

$$N = k_4 + k_5 \tag{19}$$

$$O = k_5 + k_6, \tag{20}$$

$$P = k_6 + k_7 + k_2, \tag{21}$$

$$Q = k_7 + k_8, \tag{22}$$

$$R = k_8 + k_{9f} + k_{9r}, \tag{23}$$

$$S = k_{9f} + k_{10}, \tag{24}$$

and

$$T = k_{9r} + k_{11}. \tag{25}$$

K to T represent variables in different positions of $[K]$ caused by the sum of the spring constant (k_k) as shown in Equations (16) to (25).

$\{y(t)\}$, $\{\dot{y}(t)\}$ and $\{\ddot{y}(t)\}$ represent the displacement (y_k), velocity ($\dot{y}_k$), and acceleration ($\ddot{y}_k$) vector of response, respectively, and are denoted by

$$\{y(t)\} = \left\{ \begin{array}{ccccccccccc} y_1 & y_2 & y_3 & y_4 & y_5 & y_6 & y_7 & y_8 & y_9 & y_{10} & y_{11} \end{array} \right\}^T, \tag{26}$$

$$\{\dot{y}(t)\} = \left\{ \begin{array}{ccccccccccc} \dot{y}_1 & \dot{y}_2 & \dot{y}_3 & \dot{y}_4 & \dot{y}_5 & \dot{y}_6 & \dot{y}_7 & \dot{y}_8 & \dot{y}_9 & \dot{y}_{10} & \dot{y}_{11} \end{array} \right\}^T \tag{27}$$

and

$$\{\ddot{y}(t)\} = \left\{ \begin{array}{ccccccccccc} \ddot{y}_1 & \ddot{y}_2 & \ddot{y}_3 & \ddot{y}_4 & \ddot{y}_5 & \ddot{y}_6 & \ddot{y}_7 & \ddot{y}_8 & \ddot{y}_9 & \ddot{y}_{10} & \ddot{y}_{11} \end{array} \right\}^T. \tag{28}$$

$\{F\}$ is an 11×1 force matrix whose elements are zero except those on the 10th and 11st rows which represent the sinusoidal forces given in steady state vibration. $[K_0] \in R^{11\times1}$ represents the stiffness matrix of the excitation and is denoted by

$$[K_0] = \begin{bmatrix} 0 & 0 & 0 & 0 & 0 & 0 & 0 & 0 & 0 & k_{10} & k_{11} \end{bmatrix}. \tag{29}$$

$[C_0] \in R^{11\times11}$ represents the damping matrices of the excitation and is written as

$$[C_0] = \begin{bmatrix} 0 & 0 & 0 & 0 & 0 & 0 & 0 & 0 & 0 & c_{10} & c_{11} \end{bmatrix}. \tag{30}$$

$\{y_0(t)\}$ and $\{\dot{y}_0(t)\}$ represent displacement and velocity vectors of excitation and are written as:

$$\{y_0(t)\} = \begin{Bmatrix} 0 & 0 & 0 & 0 & 0 & 0 & 0 & 0 & 0 & y_0 & y_0 \end{Bmatrix}^T \tag{31}$$

and

$$\{\dot{y}_0(t)\} = \begin{Bmatrix} 0 & 0 & 0 & 0 & 0 & 0 & 0 & 0 & 0 & \dot{y}_0 & \dot{y}_0 \end{Bmatrix}^T. \tag{32}$$

The above eleven linear differential equations are solved by computer simulation to yield $\ddot{y}_k$, $\dot{y}_k$ and y_k, ($k = 1, 2, \ldots, 11$) which are the corresponding accelerations, velocities and displacements occurring as responses to vibration waves at different frequencies. By dividing the amplitude response of each body part by its corresponding input amplitude, the amplitude ratio of that body part is computed. Similarly, the amplitude ratios of the wheelchair parts can be likewise determined. The transmissibility of different seat cushions is then determined in relation to the responses of the body parts in the 0.5 to 15[Hz] frequency range. The parameters of the body parts and wheelchair, which give the maximum vibration responses of the body parts, are listed in Tables 1 and 2.

3.2. **Frequency-domain solutions.**

3.2.1. *Frequency response analysis.* The frequency response function is analyzed using Euler's formula.

$$e^{i\omega t} = \cos\omega t + i\sin\omega t. \tag{33}$$

Euler's formula offers the agility in dealing with the real and imaginary parts of the input as well as those of the output – a capability that aids in solving the complex equations of motion. When the linear equation of motion is expressed as Equation (1), we have only the imaginary part in complex exponential form which is $\{F\}\sin\omega t = \Im[\{F\}e^{j\omega t}]$.

3.2.2. *Exponential function vectors of excitation.* The derivatives of equation of excitation from the base state are given by

$$\{y_0(t)\} = \{Y_0\}\, e^{i\omega t}, \tag{34}$$

where $\{y_0(t)\}$ represents input displacement excitation vector and $\{Y_0\}$ its corresponding magnitude.

3.2.3. *Exponential function vectors of response.* The derivatives of equation of response to vibration are given by

$$\{y(t)\} = \{Y\}e^{i\omega t}, \tag{35}$$

where $\{Y\}$ represents the magnitude of displacement vector.

3.2.4. *Exponential function vectors of all DOFs.* Input force excitation vectors on the wheelchair-occupant assembly are expressed by

$$\{F\}e^{i\omega t} = (c_{10} + c_{11})\{Y_0\}i\omega e^{i\omega t} + (k_{10} + k_{11})\{Y_0\}e^{i\omega t}, \tag{36}$$

where c_{10}, k_{10} and c_{11}, k_{11} are the damping and spring constants of the front tires (m_{10}) and rear tires (m_{11}), respectively. In Equation (36), the forces on the eleven DOFs are limited to those acting and reacting vectors according to Newton's Third Law of Motion which states, "for every force acting on a body, there is an equal and opposite reaction" [17]. For example, the FBD of the damping and spring constant of front and rear tires are derived through the following reasoning: Between the m_{10} and m_{11} masses and the ground surface, the tires would exert a stiffness force and a damping force upon the ground. The ground would respond by pushing on the tires with equal forces upward in the $y_0(t)$ direction.

3.3. **Matrix form of the complex Fourier transformation.** Fourier transformation is applied to Equations (34), (35) and (36); and the transforms then brought to substitute into Equation (1) of the steady-state response. We obtain the matrix equation for the MDOF system as

$$\left[-\omega^2[M] + i\omega[C] + [K]\right]\{Y\}e^{i\omega t} = \{F\}e^{i\omega t}. \tag{37}$$

3.4. **Solving for displacement in the complex function.** EOMs of the 11-DOF system are substituted into the complex terms in the transfer function (expressed in hertz) in Equation (1). Further manipulation of this equation enables us to eliminate the time-dependent part, thereby yielding Equation (38):

$$\frac{\{Y(i\omega)\}}{\{F(i\omega)\}} = \frac{1}{[-\omega^2[M] + i\omega[C] + [K]]}, \tag{38}$$

where $\{Y(i\omega)\}$ and $\{F(i\omega)\}$ are the corresponding complex Fourier transform vectors of $Y_k(i\omega)$ and $F_k(i\omega)$, and on the mass, damper and stiffness matrices of the body and wheelchair segments: $[M] = M_{kl}$, $[C] = C_{kl}$, and $[K] = K_{kl}$, $(k, l = 1, 2, \ldots, 11)$, as a function of ω, the excitation frequency. Upon setting the input force excitation vectors $\{F_k(i\omega)\} = F_k(i\omega)$, followed by substituting into Equation (38), we obtain the displacement values of each DOF of the body and wheelchair components as

$$\{Y_k(i\omega)\} = \frac{\{Y_k(i\omega)\}}{[-\omega^2 M_{kl} + K_{kl} + i\omega C_{kl}]}, \quad (k, l = 1, 2, \ldots, 11). \tag{39}$$

3.5. **Approaches for solving the EOMs in MDOF.** The responses from the model are evaluated against published results of experimental measurement of whole-body vibration which are adopted as our test datum. For this study, key attributes of the responses are assessed in terms of transmissibility. The proximity of the model results to the test datum is expressed as goodness-of-fit.

Next, we examine (38). The $[-\omega^2[M] + i\omega[C] + [K]]$ term therein is the impedance matrix for assessing mechanical responses from the human and vehicle frames, and it may be expressed in displacement function of vectors as shown below. $\{Y_k(i\omega)\}$ and $\{F_k(i\omega)\}$ are the corresponding complex Fourier transform vectors of $Y_k(i\omega)$ and $F_k(i\omega)$; and ω, the excitation frequency. Upon substitution in (38), we obtain

$$\{Y_k(i\omega)\} = [Q_{kl}(i\omega)]^{-1}\{F_k(i\omega)\}, \quad (k, l = 1, 2, \ldots, 11), \tag{40}$$

where $Q_{kl}(i\omega)$ is response at mass of k per unit force excitation at l. The $[-\omega^2 M_{kl} + i\omega C_{kl} + K_{kl}]$ portion has been generated by the equations of mass, damping and stiffness matrices. Its inverse, as shown in (40), becomes the impedance matrix which is $[Q_{kl}(i\omega)]$. This give us the set of matrix equations as

$$\begin{Bmatrix} Y_1(i\omega) \\ Y_2(i\omega) \\ Y_3(i\omega) \\ \vdots \\ Y_{11}(i\omega) \end{Bmatrix}$$

$$= \begin{bmatrix} Q_{11}(i\omega) & Q_{12}(i\omega) & Q_{13}(i\omega) & \dots & Q_{1(11)}(i\omega) \\ Q_{21}(i\omega) & Q_{22}(i\omega) & Q_{23}(i\omega) & \dots & Q_{2(11)}(i\omega) \\ Q_{31}(i\omega) & Q_{32}(i\omega) & Q_{33}(i\omega) & \dots & Q_{3(11)}(i\omega) \\ \vdots & \vdots & \vdots & \ddots & \vdots \\ Q_{(11)1}(i\omega) & Q_{(11)2}(i\omega) & Q_{(11)3}(i\omega) & \dots & Q_{(11)(11)}(i\omega) \end{bmatrix}^{-1} \begin{Bmatrix} F_1(i\omega) \\ F_2(i\omega) \\ F_3(i\omega) \\ \vdots \\ F_{11}(i\omega) \end{Bmatrix}, \quad (41)$$

where

$$Q_{kl}(i\omega) = \sum_{k=1}^{n}\sum_{l=1}^{n} K_{kl} + i\omega C_{kl} - \omega^2 M_{kl}, \quad (n = 1, 2, \dots, 11). \quad (42)$$

As laid out above, $[Q_{kl}(i\omega)]$, $(k, l = 1, 2, \dots, 11)$ is an 11 by 11 impedance matrix with 121 possible contributions. By using $Y_k(i\omega)$ and setting the input force vectors $F_k(i\omega) = 0$, $(k = 1, 2, \dots, 9)$; setting the front tires input $F_{10}(i\omega) = (i\omega c_{10} + k_{10})\, Y_0(i\omega)$ and rear tires input $F_{11}(i\omega) = (i\omega c_{11} + k_{11})\, Y_0(i\omega)$, followed by substituting into Equation (41), we obtain the displacement values of each DOF of the body and wheelchair components for computing the vectors and magnitudes of the displacement function in complex terms. Assuming that $[Q_{kl}(i\omega)]^{-1} = a_{kl} + b_{kl}i$ and $[Q_{kl}(i\omega)]^{-1} = c_{kl} + d_{kl}i$ are their complex values, plugging them into Equation (41) thereby yielding $\{Y_k(i\omega)\}$ as shown in Equation (43).

3.5.1. *Vectors and magnitude of the displacement function in complex terms.*

$$\begin{aligned} \{Y_k(i\omega)\} = {} & (a_{kl} + b_{kl}i)\left[(k_{10} + c_{10}(i\omega))\,\{Y_0(i\omega)\}\right] \\ & + (c_{kl} + d_{kl}i)\left[(k_{11} + c_{11}(i\omega))\,\{Y_0(i\omega)\}\right], \end{aligned} \quad (43)$$

$$\begin{aligned} |Y_k(i\omega)| = {} & \left[\sqrt{(a_{kl}^2 + b_{kl}^2)}\sqrt{\left((k_{10})^2 + (\omega c_{10})^2\right)}\right. \\ & \left. + \sqrt{(c_{kl}^2 + d_{kl}^2)}\sqrt{\left((k_{11})^2 + (\omega c_{11})^2\right)}\right] |Y_0(i\omega)|. \end{aligned} \quad (44)$$

Here $\{Y_k(i\omega)\}$ and $|Y_k(i\omega)|$ are the vectors and magnitudes of the displacement function in complex terms associated with response displacement and force excitation.

3.5.2. *Transmissibility ratio (T).* This function is defined as the ratio of the magnitudes of displacement for output response to input excitation on the wheelchair seat. It can be expressed using the above definition as

$$T = \frac{|Y_k(i\omega)|}{|Y_0(i\omega)|}, \quad (k = 1, 2, \dots, 11). \quad (45)$$

3.5.3. *Goodness-of-fit (ϵ).* For this study, key attributes of the responses are assessed in terms of transmissibility. The transmissibility results from the model are evaluated against published experimental measurements of whole-body vibration which serve as our test datum. The proximity of the model results to the test datum is expressed as goodness-of-fit whose expression is shown in Equation (46) [16]:

$$\epsilon = 1 - \frac{\sqrt{\frac{\sum_{m=1}^{N}(\tau_m - \tau_c)^2}{N-2}}}{\frac{\sum_{m=1}^{N}\tau_m}{N}}. \tag{46}$$

In Equation (46), τ_m is the test datum, τ_c is the calculated result from each model, and N is the number of test data points used in the comparison. As the value of ϵ moves towards 1, the predicted results approach a perfect fit with the published data.

4. Results and Discussion.

4.1. **Biodynamic evaluation of the wheelchair-occupant model.** Preliminary validation of our model was carried out by first determining its response in terms of head-to-pelvis displacements associated with a set of pre-selected input parameters. The predicted values from the model could then be checked against published, real-world results. Figure 2 shows the predicted head-to-pelvis displacement ratios as a function of input frequency obtained from our model according to the input parameters we employed, which are listed in Tables 1 and 2.

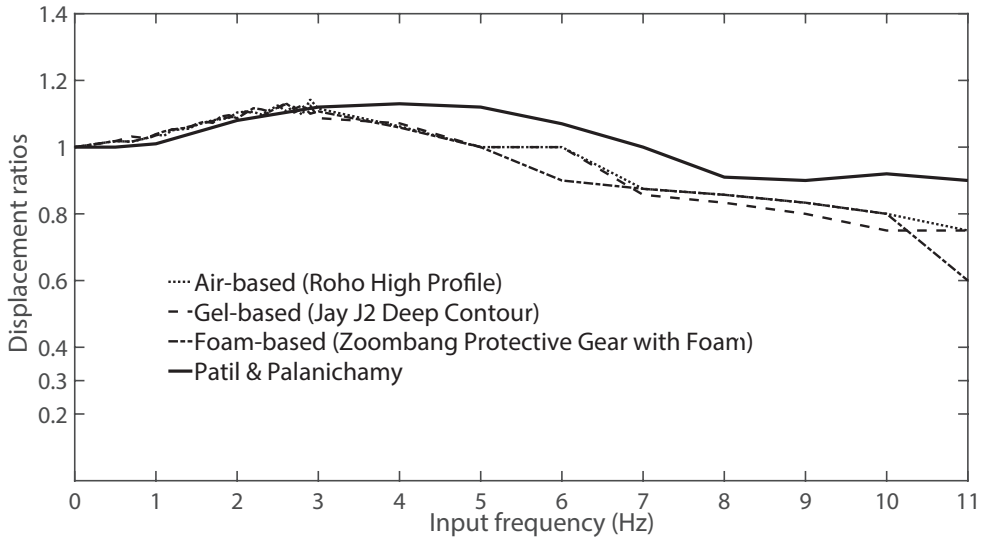

FIGURE 2. Head-to-pelvis displacement ratios obtained in tests with air-, gel- and foam-based cushions

As shown in Figure 2, the first peak of displacement ratios occurs at the frequency approximately 3[Hz]. Superimposed thereon is the experimental curve for the same attribute derived by Patil and Palanichamy [18], which is seen to nearly match the curves from our model runs. Hence, the test results confirm our work as a quality composite model since good agreement is found between it and corresponding real-world findings reported in industry literature and the ISO recommendations cite in [19].

4.2. **Comparison of seat transmissibility results via goodness-of-fit.** This is the comparison of transmissibility results obtained from the model with those from real-world experiments through the use of a mathematical test known as goodness-of-fit. Figure 3 and Table 3 show the measured values obtained from actual wheelchair road course (WRC) tests [9] which define the region for the seat transmissibility in comparison with the values predicted by our model.

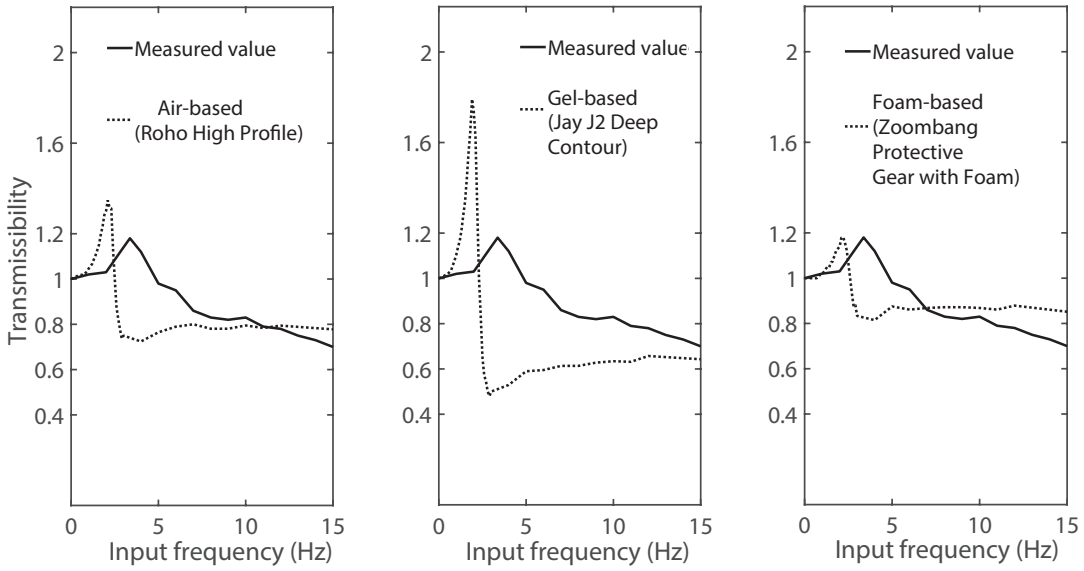

FIGURE 3. Comparison between measured and predicted values of seat transmissibility for three seating systems

TABLE 3. Peak transmissibility ratios (T) and corresponding frequency (f, *in* [Hz]) from actual wheelchair road course (WRC) test [9], and results from 11-DOF model runs

Cushion	WRC		11-DOF	
	f	T	f	T
Air-based	3.37	1.18	2.1	1.36
Gel-based	3.48	0.99	1.9	1.78
Foam-based	3.36	1.13	2.1	1.17

TABLE 4. Goodness-of-fit (ϵ) results of transmissibility ratios from model runs

Attribute	Cushion		
	Air-based ϵ	Gel-based ϵ	Foam-based ϵ
Transmissibility	0.76	0.58	0.84

Table 3 summarizes the peak transmissibility values and their corresponding frequencies. While Columns T of the WRC and the 11-DOF tests show comparable peak measurements, the frequencies at which the peaks occur, listed under Columns f, show wide discrepancies. A possible reason for such differences could be that the 11-DOF model was formulated to fit seat transmissibility data obtained by directly vibrating the simulated occupant with harmonic input excitation over the range 1 to 15[Hz], whereas the frequency content of the vibration produced by the road course on the human subject was variable on a wider range. The peak transmissibility values of the WRC and 11-DOF tests were assessed for goodness-of-fit using Equation (46); and the results laid out in Table 4. According to Table 4, the values predicted by our model are largely in good proximity to the real-world results from the WRC test, and the best goodness-of-fit achieved is 84[%] for the foam-based cushion.

Thus, the vibration transmissibility given out by our model is found to correlate well with real-world experimental results, indicating the potential role of mathematical modelling as a tool to aid wheelchair cushion design. In this study, the foam-based cushion

outperformed the gel- and air-based options and should be considered by clinicians when selecting a cushion to help protect the wheelchair rider from the detrimental effects of whole-body vibration.

4.3. **Displacement response obtained from simulation runs.** Results in Figures 4 to 5 and Table 5 show the resulting amplitudes of displacement associated with the body segments supported on three cushion types. The torso (y_3) exhibits the largest shock of 0.0167[m] at 1.5[Hz] on the gel-based cushion while the pelvis (y_7) receives the smallest shock of 0.0131[m] at 1.6[Hz] on the foam-based pad. For all the mass segments in the study, the maximum displacement magnitude occurs at frequency 1.6[Hz] for the foam-based and air-based cushions; and at 1.5[Hz] for the gel-based pad [20]. For the body parts, the resultant displacement responses peak at the frequency range of 1.5 to 1.6[Hz].

TABLE 5. Amplitudes of displacement (y, *in* [m]), at resonance frequency (f, *in* [Hz]), obtained from the model's body parts in tests with air-, gel- and foam-based cushions

Body part	Peak displacement		
	Air-based ($y, f = 1.6$)	Gel-based ($y, f = 1.5$)	Foam-based ($y, f = 1.6$)
Head (y_1)	0.0146	0.0161	0.0141
Back (y_2)	0.0145	0.0160	0.0140
Torso (y_3)	0.0151	0.0167	0.0146
Thorax (y_4)	0.0150	0.0165	0.0145
Diaphragm (y_5)	0.0148	0.0164	0.0143
Abdomen (y_6)	0.0145	0.0161	0.0140
Pelvis (y_7)	0.0136	0.0151	0.0131

For solutions that describe the behavior of a mass (m_1 to m_8) per unit input force as a function of frequency, y_1 to y_8 are the resulting displacements or magnitudes of the model response; while y_0 the displacement which is the base magnitude of excitation. Upon examination of the responses of displacement curves obtained from model runs for all eight cases – head, back, torso, and so on – and the resulting displacement magnitudes with the three cushion types, it was found that the foam-based cushion produced the smallest values of displacement. This is laid out in Table 5. Note that among the three brands, the foam-based has the largest spring stiffness constants. If we take the body-part response to excitation, and divide it with the input displacement excitation, $y_0(i\omega)$, we can observe the interaction of the parameters. If the stiffness constant is raised, the magnitude of displacement will decrease, but the related position of frequency will increase as a consequence due to the change in natural frequency of the system.

Examination of the displacement profiles reported in the works of [14] and [18] revealed that the body-part responses to vibration in their respective experiments are very similar. Furthermore, their results are replicated by our 11-DOF model as shown in Figures 4 and 5 with the torso being the most responsive, i.e., outputting the largest displacement values; while the pelvis, the least vulnerable. As shown in Figures 4 and 5, the gel-based pad gave out the largest magnitudes of displacement within the input frequency range 0.5 to 1.5[Hz], and almost zero magnitude as the input frequency rose beyond 1.6[Hz]. Similarly, with the air- and foam-based types, their displacement responses peaked within the frequency range 0.5 to 1.6[Hz], and dropped to near zero beyond 1.7[Hz].

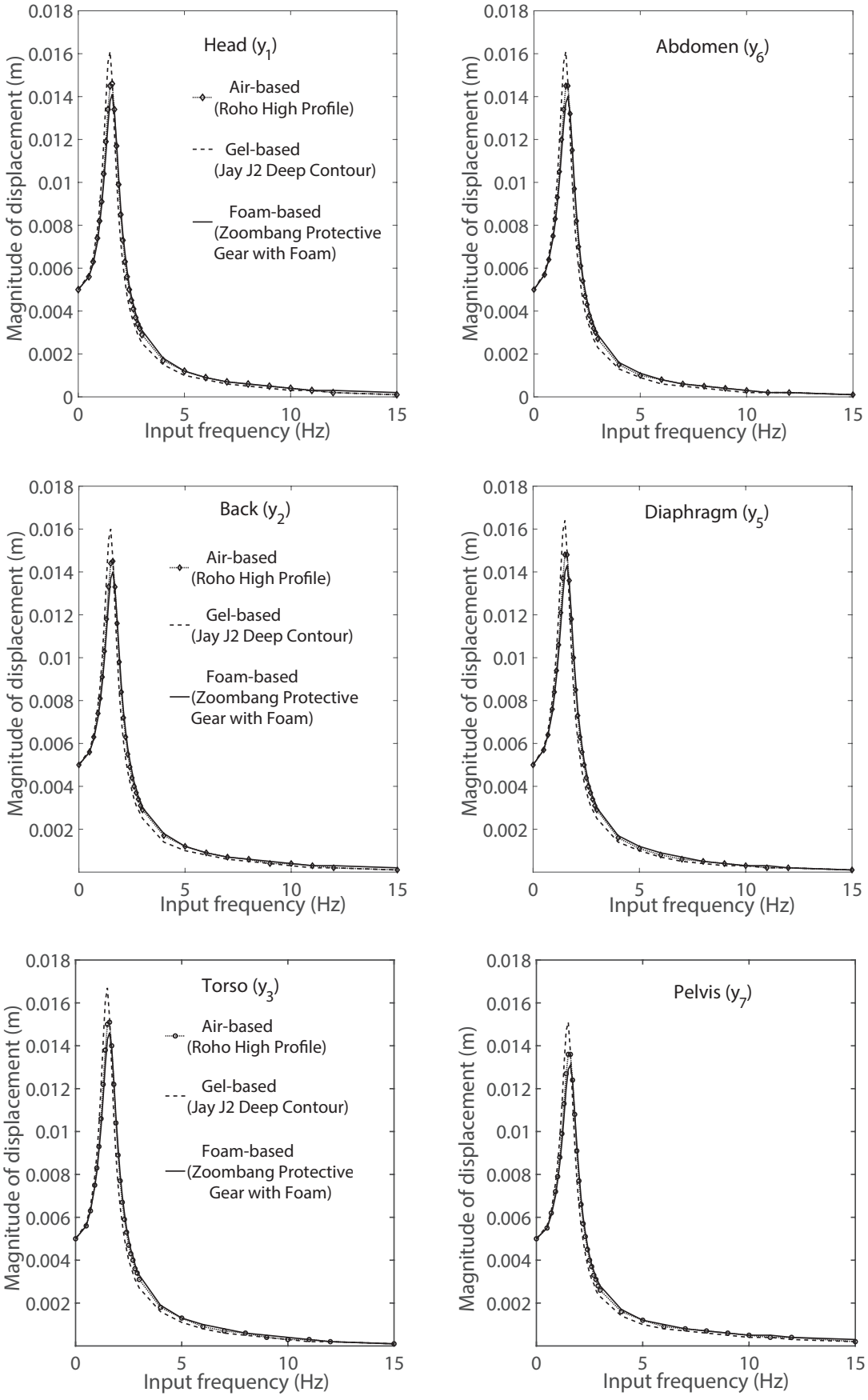

FIGURE 4. Amplitudes of displacement exhibited by the model's body parts in tests with the three cushion types

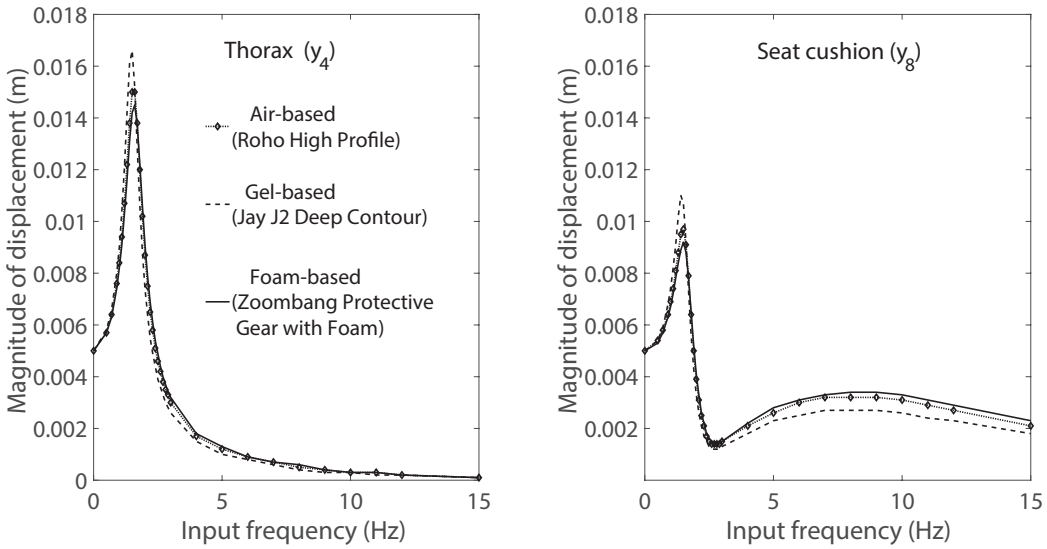

FIGURE 5. Amplitudes of displacement exhibited by the model's thorax and seat cushions

The model's response as seen in this study provides the assurance that cushion parameters are essential for characterizing vibration and should be considered in the engineering of the wheelchair seat in order to provide better ride comfort [21, 22]. The model in this study has two resonance frequencies and an absolute maximum displacement. i) We consider the magnitude of frequency response that should change across the frequency range upon any change in seat parameters. It should be noted that at the low end of excitation frequency, the response exhibited is roughly k. Therefore, if we want to reduce this magnitude of frequency response, then we would need to decrease the stiffness constant (making k smaller). ii) Whenever a peak reduction is desired, increases in the damping constant should thus be considered. This means that damping control is key to controlling an absolute maximum displacement.

When results deriving from all the cushion types are listed in descending order, it is found that the cushion types with lower damping constants would yield higher displacement values and, conversely, those with higher damping constants would produce smaller displacements as shown in Figures 4 to 5 and Table 5. In a real-life situation, input excitation originates from the floor, spreads to and subjects the wheelchair in vibration. The fundamental approach to reducing such vibration on the wheelchair has the following steps: i) change the properties of the system; ii) change its natural frequency and iii) adjust its damper setup [2, 23]. Regular device monitoring is required for a proper maintenance routine, and when necessary, the device should be taken out of use or repairs administered. A simple solution worth considering is changing or adding a suitable seat cushion, which generally could be carried out without incurring too high a cost.

5. **Conclusions.** Results from our 11-DOF model show that, with the three cushion types tested, they managed to closely mimic the results of well-defined real-world experiments as measured by their having a satisfactory goodness-of-fit. The response of the occupant's torso within the test frequency range has the highest amplitudes of displacement relative to that exhibited by other body segments. By contrast, the pelvis has the least displacement response. Vibration effects transmitted from the cushions are found to be the lowest with the foam-based type, thus signifying its superior shock absorbing behavior to that of the air-based and gel-based options. However, only slight differences in amplitude value are seen in Table 5; and such slight differences alone are not significant

enough for us to rate the materials. However, if we also take account of a material's ease of maintenance as well as its lower cost, then the winning position of the foam-based cushion is amply justified. Further research in this area may be in order, especially in improving cushion design so as to achieve further reduction of the vibration arising from the uneven contact between ground and wheelchair. This may be affected by using suitable target values of dynamic stiffness and damping constant that would yield better seat displacement response applicable to increasing human ride comfort.

Acknowledgment. This material is the result of work supported by JSPS KAKENHI Grant Number JP21K03930 and the Royal Thai Government Scholarship.

REFERENCES

[1] M. L. Toro-Hernández, L. Alvarez, M. C. Vargas-Chaparro and M. Goldberg, Final year students' knowledge on basic manual wheelchair provision: The state of occupational therapy programs in Colombia, *Occupational Therapy International*, vol.2020, pp.1-8, 2020.

[2] O. Lariviere, D. Chadefaux, C. Sauret and P. Thoreux, Vibration transmission during manual wheelchair propulsion: A systematic review, *Vibration*, vol.4, pp.444-481, 2021.

[3] Y. Garcia-Mendez, J. L. Pearlman, M. L. Boninger and R. A. Cooper, Health risks of vibration exposure to wheelchair users in the community, *Journal of Spinal Cord Medicine*, vol.36, pp.365-375, 2013.

[4] M. J. Griffin, Discomfort from feeling vehicle vibration, *Vehicle System Dynamics*, vol.45, pp.679-688, 2007.

[5] J. Gao, A. Sha, Y. Huang, L. Hu, Z. Tong and W. Jiang, Evaluating the cycling comfort on urban roads based on cyclists' perception of vibration, *Journal of Cleaner Production*, vol.192, pp.531-541, 2018.

[6] S. N. W. Vorrink, L. H. V. Van der Woude, A. Messenberg, P. A. Cripton, B. Hughes and B. J. Sawatzky, Comparison of wheelchair wheels in terms of vibration and spasticity in people with spinal cord injury, *Journal of Rehabilitation Research & Development*, vol.45, pp.1269-1280, 2008.

[7] F. Chnier and R. Aissaoui, Effect of wheelchair frame material on users' mechanical work and transmitted vibration, *Biomedical Research*, vol.2014, pp.1-12, 2014.

[8] T. Waga, S. Ura, M. Nagamori, H. Uchiyama and A. Shionoya, Influence of material on wheelchair vibrations, *The 13th Conference of the International Sports Engineering Association*, pp.1-6, 2020.

[9] Y. Garcia-Mendez, J. L. Pearlman, R. A. Cooper and M. L. Boninger, Dynamic stiffness and transmissibility of commercially available wheelchair cushions using a laboratory test method, *Journal of Rehabilitation Research & Development*, vol.49, no.1, pp.7-22, 2012.

[10] M. Ferguson-Pell, G. Ferguson-Pell, F. Mohammadi and E. Call, Applying ISO 16840-2 standard to differentiate impact force dissipation characteristics of selection of commercial wheelchair cushions, *Journal of Rehabilitation Research & Development*, vol.52, pp.41-52, 2015.

[11] C. Zhou, Y. Shen and Z. Wang, Research on vibration suppression of transmission chain in wind power generation system with gear clearance based on internal model control, *International Journal of Innovative Computing, Information and Control*, vol.18, no.4, pp.1247-1263, 2022.

[12] P. Weerapong, K. Hashikura, M. A. S. Kamal and K. Yamada, A model for the response of an occupant and wheelchair system subjected to vertical vibrations, *International Journal of Innovative Computing, Information and Control*, vol.17, no.6, pp.1823-1841, 2021.

[13] P. Weerapong, K. Hashikura, M. A. S. Kamal and K. Yamada, A biodynamic model of wheelchair with changeable seat cushions subjected to vertical vibrations, *ICIC Express Letters*, vol.16, no.1, pp.33-41, 2022.

[14] J. D. Quadros, P. Suhas and N. L. Vaishak, A numerical study for determining the ideal operating speed for a two-wheeler rider on varying terrain amplitudes, *Journal of Mechanical Science and Technology*, vol.30, pp.2435-2442, 2016.

[15] M. F. Hikmawan and A. S. Nugraha, Analysis of electric wheelchair passenger comfort with a half car model approach, *ICSEEA 2016 International Conference on Sustainable Energy Engineering and Application*, pp.76-80, 2016.

[16] C. C. Liang and C. F. Chiang, A study on biodynamic models of seated human subjects exposed to vertical vibration, *International Journal of Industrial Ergonomics*, vol.36, pp.869-890, 2006.

[17] P. Cornille, Review of the application of Newton's Third Law in physics, *Progress in Energy and Combustion Science*, vol.25, pp.161-210, 1998.
[18] M. K. Patil and M. S. Palanichamy, A mathematical model of tractor-occupant system with a new seat suspension for minimization of vibration response, *Applied Mathematical Modelling*, vol.12, pp.63-71, 1988.
[19] ISO Standard 2631-5, *Mechanical Vibration and Shock – Evaluation of Human Exposure to Whole-Body Vibration. Part 1: General Requirements*, International Organization for Standardization, Geneva, 2018.
[20] P. Weerapong, K. Hashikura, M. A. S. Kamal and K. Yamada, A numerical study of model output for whole-body vibration on varying wheelchair cushions, *The 7th International Conference on Business and Industrial Research*, 2022.
[21] H. T. Bui, L. V. Nguyen, K. Debray, Q. B. Tao and P. Lestriez, Modeling and experimental of the mechanical behavior of seat cushion for wheelchair users, *IOP Conference Series: Materials Science and Engineering*, pp.1-8, 2019.
[22] Y. A. Wicaksono, L. Herdiman and S. Susmartini, Cushion seat design on manual wheelchair for people with paralysis using value engineering method to improve activity comfort: A preliminary study, *Journal of Physics: Conference Series*, vol.1450, no.1, pp.1-9, 2020.
[23] Z. Dziechciowski and M. Kromka-Szydek, Vibration transmitted to the human body during the patient's ride in a wheelchair, *Archives of Acoustics*, vol.42, no.1, pp.137-148, 2017.

Author Biography

Pongtep Weerapong received the B.E. degree in Materials Engineering, 2005; the M.E. degree in Polymer Processing Engineering, 2007 from King Mongkut's University of Technology Thonburi (KMUTT), Thailand.

Mr. Weerapong is currently a doctoral candidate in Mechanical Science and Technology at Gunma University, Japan. His research interests include assistive technology for children with disabilities and whole-body vibration.

Kotaro Hashikura received the B.S. degree in Mechanical Engineering from Kyushu Institute of Technology, Fukuoka, Japan, 2006; the M.S. degree of Informatics from Kyoto University, Kyoto, Japan; 2010, and the Doctor Degree in Engineering from Tokyo Metropolitan University, Tokyo, Japan, 2014. From 2014 until 2018, he had been a Project Research Associate at the Faculty of System Design, Tokyo Metropolitan University.

Prof. Hashikura is currently a full-time professor at Division of Mechanical Science and Technology, Gunma University, Japan. His research interests include time-delay-related control techniques, such as deadbeat, preview-prediction and repetitive controls. He is a member of IEEE, ISCIE and SICE.

Md Abdus Samad Kamal received the B.Sc. degree in Electrical and Electronic Engineering from Khulna University of Engineering and Technology (KUET), Khulna, Bangladesh in 1997; Master and Doctor degrees from Kyushu University from Graduate School of Information Science and Electrical Engineering, Japan in 2003 and 2006, respectively. He was a post-doctoral fellow in Kyushu University till November 2006.

Prof. Kamal is currently a full-time professor at Division of Mechanical Science and Technology, Gunma University, Japan. His current research interests are reinforcement learning, intelligent transportation systems, and multiagent systems.

Iwanori Murakami received the B.E., M.E. and Dr. Eng. degrees from Gunma University, Kiryu City, Japan, in 1992, 1994 and 1997, respectively.

Prof. Murakami is currently a full-time professor at Division of Mechanical Science and Technology, Gunma University, Japan. His research interests include control problems in the mechanical fields and robotics.

Kou Yamada received B.S. and M.S. degrees in Electrical and Information Engineering from Yamagata University, Yamagata, Japan, 1987 and 1989, respectively; and the Dr. Eng. Degree from Osaka University, Osaka, Japan in 1997.

Prof. Yamada is currently a full-time professor at Division of Mechanical Science and Technology, Gunma University, Japan. His research interests include robust control, repetitive control, process control and control theory for inverse systems and infinite-dimensional systems. Dr. Yamada received the 2005 Yokoyama Award in Science and Technology, the 2005 Electrical Engineering/Electronics, Computer, Telecommunication, and Information Technology International Conference (ECTI-CON2005) Best Paper Award, the Japanese Ergonomics Society Encouragement Award for Academic Paper in 2007, the 2008 Electrical Engineering/Electronics, Computer, Telecommunication, and Information Technology International Conference (ECTI-CON2008) Best Paper Award and 4th International Conference on Innovative Computing, Information and Control Best Paper Award in 2009, the 14th International Conference on Innovative Computing, Information and Control Best Paper Award in 2019 and Outstanding Achievement Award from Kanto Branch of Japanese Society for Engineering Education in 2022.